## Distributed Current Injection into a One-Dimensional Ballistic Edge Channel

Kristof Moors, 1.2,\*,‡ Christian Wagner, 3 Helmut Soltner, 4 Felix Lüpke, 2,3,5

F. Stefan Tautz, 3,2,6,† and Bert Voigtländer, 52425 Jülich, Germany

1 Peter Grünberg Institute (PGI-9), Forschungszentrum Jülich, 52425 Jülich, Germany

2 Jülich Aachen Research Alliance (JARA), Fundamentals of Future Information Technology, 52425 Jülich, Germany

3 Peter Grünberg Institute (PGI-3), Forschungszentrum Jülich, 52425 Jülich, Germany

4 Institute of Technology and Engineering (ITE), Forschungszentrum Jülich, 52425 Jülich, Germany

5 Institute of Physics II, Universität zu Köln, Zülpicher Straße 77, 50937 Köln, Germany

6 Experimental Physics IV A, RWTH Aachen University, Otto-Blumenthal-Straße, 52074 Aachen, Germany

(Received 26 February 2025; accepted 23 September 2025; published 29 October 2025)

We generalize Landauer's theory of ballistic transport in a one-dimensional (1D) conductor to situations where charge carrier injection and extraction are not any more confined to electrodes at either end of the channel, but may occur along its whole length. This type of distributed injection is expected to occur from the two-dimensional (2D) bulk of, e.g., a quantum spin (or anomalous) Hall insulator to its topologically protected edge states. We apply our conceptual solution to the case of two metal electrodes contacting the 2D bulk, enabling us to derive criteria that discriminate ballistic from resistive edge channels in multiterminal transport experiments.

DOI: 10.1103/I47r-plxq

Charge transport through a 1D channel without scattering was famously explained by Rolf Landauer decades ago [1–3]. He considered a ballistic conductor between two metal electrodes, with charge carrier injection at one end and extraction at the other [Fig. 1(a)]. Importantly, in Landauer's seminal work neither injection nor extraction is allowed along the length of the channel. This situation is realized, e.g., in 2D electron gases in GaAs-AlGaAs heterostructures [4,5] and carbon nanotubes [6], for which Landauer's theory has provided accurate predictions.

With the recently rising interest in topologically protected edge channels in quantum spin or anomalous Hall systems (semiconductor quantum wells [7–13], 2D materials [14–24], and graphene nanoribbons [25,26]), a fundamentally different experimental situation has moved into focus: the ballistic channel exists alongside a 2D half-plane with which it forms an interface along the complete channel length; beyond this extended interface contact, there are no further specific injection contacts. If, as is the case in most experimental realizations of the systems mentioned above, the half-plane has a nonvanishing residual conductivity, any

Contact author: s.tautz@fz-juelich.de Contact author: kristof.moors@imec.be

Published by the American Physical Society under the terms of the Creative Commons Attribution 4.0 International license. Further distribution of this work must maintain attribution to the author(s) and the published article's title, journal citation, and DOI. voltage applied within the half-plane will cause a current injection into the ballistic channel that is distributed along the length of the channel. Clearly, this set of circumstances is not covered by Landauer's original considerations [1–3].

Here, we generalize Landauer's theory of ballistic transport to the situation of distributed injection into a 1D channel. To this end, we specify an injection (and extraction) current density distribution in the 2D half-plane and solve the transport problem from the fundamental principle of conductance quantization in the 1D channel with perfect transmission (conductance  $G_0/2 = e^2/h \approx (25.8 \text{ k}\Omega)^{-1}$  per spin, e.g., Ref. [27]). We consider the transport in the contacts (here: the 2D half-plane) as diffusive and thus employ a semiclassical approach based on Poisson's equation [28], rather than a fully self-consistent quantum mechanical treatment [29,30].

Beyond formulating a conceptual, geometry-independent framework for distributed injection, we solve a specific class of injection geometries—symmetrically placed pointlike injection contacts in the half-plane. This geometry is directly applicable to nanoprobes and multitip scanning tunneling microscopy (STM), powerful experimental methods to study 2D transport at the nanoscale [31]. Using the explicit solution provided here, multiterminal potentiometry [32] can overcome the challenge to discriminate topological (ballistic) from trivial (diffusive) edge channels, which is impossible in single-tip STM, because in both cases the vertical tunneling conductivity can be enhanced by the high local density of states near the edge [16,17,24,33–36].

Contact geometry—For current injection into the conducting 2D half-plane with sheet conductivity  $\sigma$ , we

<sup>\*</sup>Present address: Imec, Kapeldreef 75, 3001 Leuven, Belgium.

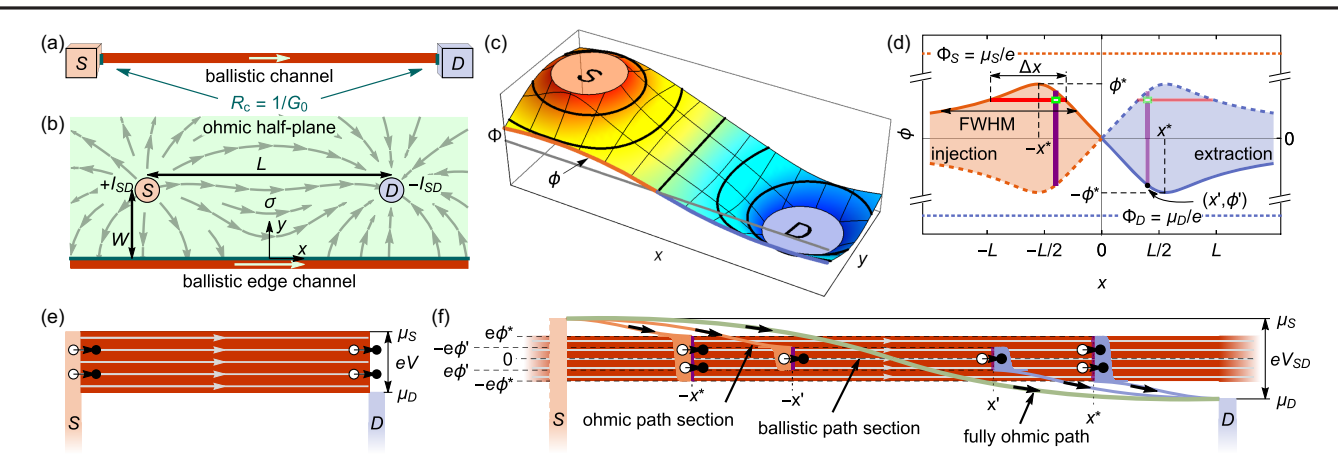


FIG. 1. 1D ballistic edge channel with distributed injection. (a) In the standard Landauer setup, charge carriers are injected and extracted locally at the ends of a 1D ballistic channel. The contact resistance at each contact (indicated by the teal interfaces) is  $R_c = 1/G_0$  per spin. (b) In the contact geometry considered here, current enters and exits a 1D ballistic edge channel in a distributed manner via a conducting half-plane with sheet conductivity  $\sigma$  and symmetrically positioned source (S) and drain (D) contacts (e.g., STM tips). (c) Potential  $\Phi(x, y)$  in the 2D half-plane, obtained by solving the Poisson equation with boundary condition  $\Phi(x, y = 0^+) = \phi(x)$  at the interface with the 1D ballistic channel. The interface potential  $\phi(x)$ , indicated as solid orange (blue) lines on the source (drain) side, is obtained by numerically solving the filling condition. (d) The antisymmetric  $\phi(x)$  (see text for details). (e) Energy diagram of charge carrier transport in the standard Landauer setup shown in (a). (f) Energy diagram for the contact geometry shown in (b).

consider small circular source (S, potential  $\Phi_S = \mu_S/e$ ) and drain (D, potential  $\Phi_D = \mu_D/e$ ) contacts [Fig. 1(b)]. This situation can be realized, for instance, with small lithographic contacts or by contacting two tips of a multitip STM to a sample surface [28,31,37,38]. Source and drain are positioned at a distance L from each other and a common distance W from the ballistic channel. For the configuration in Fig. 1(b), the whole region x < 0, y = 0 can be considered as the region of distributed injection from the source contact into the 1D ballistic channel and, correspondingly, the region x > 0, y = 0 as the region of distributed extraction towards the drain contact.

Distributed injection—In the situation displayed in Fig. 1(b), a current distribution develops over the halfplane with different types of current paths from source to drain: (i) fully Ohmic paths that do not enter the ballistic channel and (ii) paths that go via the ballistic channel, thereby including both resistive and ballistic sections. The current paths can be obtained from a continuously varying potential  $\Phi(x, y)$  whose profile is governed by the Poisson equation  $[\nabla^2 \Phi(x, y) = -\nabla \cdot \mathbf{j}/\sigma]$  with appropriate boundary conditions for the contacts and the interface with the ballistic channel at y = 0. We consider, without loss of generality, antisymmetric boundary conditions at the contacts, giving rise to an antisymmetric potential along x,  $\Phi(x,y) = -\Phi(-x,y)$ . The boundary condition for the potential at the interface to the ballistic channel depends on the latter's properties (more specifically, the filling of its states) which will be discussed below. It results in an interface potential profile  $\Phi(x, y = 0^+) \equiv \phi(x)$ , the generic shape of which, including a single maximum  $\phi^*$ and  $\phi(x) = -\phi(-x)$  [see solid orange and blue lines in Figs. 1(c) and 1(d)], follows from symmetry considerations (Supplemental Material Note 1 [39]).

Utilizing the generic  $\phi(x)$  in Fig. 1(d), we discuss charge carrier injection into and extraction out of the ballistic channel with the help of Figs. 1(e) and 1(f). In Landauer's treatment, a source reservoir injects right movers from an energy window  $[\mu_D, \mu_S]$  into the ballistic channel [Fig. 1(e)], corresponding to a bias voltage  $V = \Phi_S - \Phi_D = (\mu_S - \mu_D)/e$ (here considering positive charge carriers and V > 0 for convenience, without loss of generality). For the ballistic channel to exhibit a perfectly quantized conductance, all available right moving states in the channel must be occupied through the injection in this energy window and propagate with perfect transmission between source and drain, without being compensated by states moving in the opposite direction (reflectionless drain contact) [27]. In contrast, in the distributed contact geometry the energy window for injection becomes a function of x, as shown by the orange shaded region in Fig. 1(d). On each Ohmic current path section between source contact and ballistic channel, carriers lower their energy by  $\mu_S - e\phi(x)$  [light orange paths with arrows in Fig. 1(f) for two different values of x]. This yields  $e\phi(x)$  as a local upper limit for the energy of carriers injected at x into the ballistic channel on the source side (x < 0), shown as a solid orange line in Fig. 1(d). A similar argument applies to the carriers extracted on the drain side (x > 0) that lower their energy by  $e\phi(x) - \mu_D$  [light blue paths in Fig. 1(f)] between the ballistic channel and the drain contact. As they can only enter the drain contact with energy  $\mu_D$  or higher, the lower energy limit to exit the ballistic channel at x > 0 is  $e\phi(x)$ [solid blue line in Fig. 1(d)]. Dictated by symmetry, corresponding injection and extraction paths, arriving at the ballistic channel at x < 0 and departing from it at -x > 0, respectively, feature the same energy loss in the 2D plane. As a consequence, the energy distribution of injected charge carriers at x < 0 must be identical to that of the extracted carriers at -x > 0. This implies that the upper (lower) limit for injection (extraction) at x < 0 (x > 0) is also the upper (lower) limit of extraction (injection) at -x > 0 (-x < 0), shown as dashed blue (orange) line in Fig. 1(d) (Supplemental Material Note 2 A [39]). Hence, at all x, injection and extraction windows at the ballistic channel are spread symmetrically around zero energy with width  $2e|\phi(x)|$  and symmetric around x = 0 [see orange and blue shaded regions in Fig. 1(d)].

When charge carriers enter the ballistic channel, they leave holes behind in the Ohmic 2D plane [indicated by white circles at positions  $-x^*$  and -x' in Fig. 1(f)]. These holes are highly energetic compared to the surrounding Fermi sea and quickly filled by dissipative relaxation processes in the 2D Ohmic plane within a short distance  $\lambda_{\rm mfp}$ , as indicated by orange areas close to the interface in Fig. 1(f). We consider  $\lambda_{\rm mfp} \ll |\Phi_S|/|\nabla\Phi|$ , L, W such that conventional Ohmic transport with sheet conductivity  $\sigma$  is effectively maintained in the half-plane and  $\lambda_{\text{mfp}}$  does not enter our solutions explicitly (Supplemental Material Note 2 C [39]). Analogous processes occur when charge carriers exit the ballistic channel. Together, these relaxation processes add to the overall dissipation for a path from the source to the drain electrode via the ballistic channel, such that the total dissipation is equal to  $\mu_S - \mu_D$  for all current paths  $[2e|\phi(x')|$  occurring within  $\lambda_{\mathrm{mfp}}$  of the interface to the channel, and  $\mu_S - \mu_D - 2e|\phi(x')|$  spread over the entire path through the 2D half-plane, for a current path with entry point -x' and exit point x'].

Filling condition—To retain a perfectly quantized ballistic channel in our setup, all right moving states in the energy interval  $[-e\phi^*, +e\phi^*]$  around the equilibrium chemical potential must be completely occupied and propagate with perfect transmission between the regions of distributed injection and extraction, while obeying the local limits regarding the injection or extraction energies as discussed in the previous section. Implementing these requirements by equating the local current density entering the ballistic channel from the 2D half-plane to the complete filling of its states over all energies that are locally accessible, we obtain the filling condition

$$\left. \sigma \partial_y \Phi(x, y) \right|_{y=0^+} = \frac{G_0}{2} \int_{-\phi(x)}^{\phi(x)} d\phi \frac{1}{\Delta x(\phi)}. \tag{1}$$

The right-hand side is a Riemann-Stieltjes integral from  $-\phi(x)$  to the local potential  $\phi(x)$  [vertical purple stripes in Figs. 1(d) and 1(f)]. Note that the equation is nonlocal, as the injection to completely fill the density of states of the ballistic channel at each energy  $e\phi$  is distributed over the length  $\Delta x(\phi)$  [horizontal red stripe in Fig. 1(d)]. The interface potential  $\phi(x)$  together with the boundary conditions for the contacts uniquely determine the potential

landscape  $\Phi(x, y)$  over the complete half-plane via analytical continuation and thereby also fix the injected current density on the left-hand side of Eq. (1). Examples for the numerically calculated  $\Phi(x, y)$  and  $\phi(x)$  are shown in Figs. 1(c) and 2(a), respectively. The derivation of Eq. (1) and the numerical method for solving it [42] are provided in Supplemental Material Notes 2 A and B [39]. We stress that the filling condition follows from general considerations (current continuity, energy conservation, symmetry) within semiclassical transport theory applied to the (ideally insulating) half-plane in the presence of residual charge carriers and ballistic transport without scattering in the edge channel [44], thereby avoiding a self-consistent Schrödinger-Poisson treatment of electron density and potential in the mixed 1D-2D system [29,30]. We further emphasize that  $\phi(x)$  from Eq. (1) is expected to peak in the range 1.5 to 15 mV for typical parameters (Supplemental Material Note 4), well within the resolution of, e.g., STM-based potentiometry and therefore directly accessible in experiment.

Comparison to quasi-1D resistive channels—To evaluate the distinct transport behavior of a ballistic channel, we compare the interface potential  $\phi(x)$  as obtained from the filling condition [Eq. (1)] with the interface potential of a quasi-1D Ohmic channel [45]. The latter is modeled as a narrow stripe of width  $d \ll W$ , L, with  $y \in [-d, 0]$  and infinite extension along x, having a sheet conductivity  $\sigma_{\rm O}$ (1D conductivity  $\sigma_{\Omega}d$ ); its potential can be obtained analytically (Supplemental Material Note 3 [39]) and has the same generic shape as that of a ballistic channel [Fig. 2(a)]. Natural limiting cases are the perfectly conducting Ohmic channel  $(\sigma_{\Omega} \to \infty)$ , with vanishing interface potential ( $\phi = 0$ ) and maximal current, and the fully insulating Ohmic channel  $(\sigma_{\Omega} \to 0)$  carrying zero current.  $\phi_{\sigma_0 \to 0}$  provides a convenient upper limit, since any finite current injection naturally lowers the interface potential towards zero (the opposite limiting case). Hence, we normalize all interface potentials with  $\phi_{\sigma_0 \to 0}^*$ , the maximum of  $\phi_{\sigma_0 \to 0}(x)$ .

To explore whether the interface potential of a ballistic channel ( $\phi_{\text{ball}}$ ) can be emulated by an Ohmic channel, we choose the latter's sheet conductivity  $\sigma_{\Omega_1}$  to match the quantized conductance  $G_0/2$  over the length L, i.e.,  $\sigma_{\Omega_1} \equiv (G_0/2)L/d$ . While the interface potentials  $\phi_{\text{ball}}$ and  $\phi_{\Omega_1}$  [Fig. 2(a)] appear qualitatively similar, there are notable differences:  $\phi_{\Omega_1}$  exhibits a slower decay at large |x| > L, but a gentler slope towards x = 0, with a crossover of the interface potentials around  $|x| \sim L/2$ . These differences arise because the voltage drop of an Ohmic channel scales with the path length, while being path length independent over a ballistic channel. Adjusting the sheet conductivity of the Ohmic channel, some features of  $\phi_{\text{ball}}$ can be recovered more accurately. However, systematic agreement with  $\phi_{\mathrm{ball}}$  along the whole interface cannot be obtained for any quasi-1D Ohmic channel.

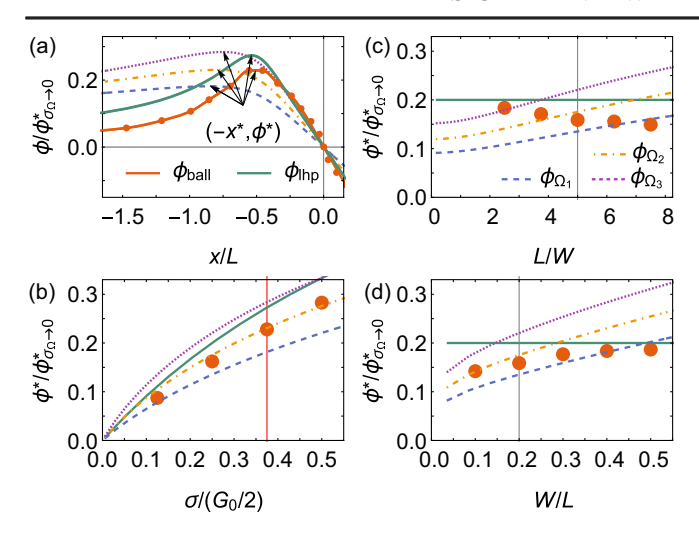


FIG. 2. Normalized interface potential  $\phi_{\rm ball}$  of a 1D ballistic edge channel (solid orange line and orange circles), in comparison with several resistive proxies: quasi-1D Ohmic channels  $\Omega_1$  with  $\sigma_{\Omega_1}=(G_0/2)L/d=3874~\mu {\rm S}\Box^{-1}$  (dashed blue),  $\Omega_2$  with  $\sigma_{\Omega_2}=0.7\sigma_{\Omega_1}$  (dash-dotted yellow),  $\Omega_3$  with  $\sigma_{\Omega_3}=0.5\sigma_{\Omega_1}$  (dotted purple), and Ohmic lower half-plane with  $\sigma_{\rm lhp}=G_0/2$  (solid green), (a) as a function of x with  $L=1~\mu {\rm m},~W=0.2~\mu {\rm m},~\sigma=0.375G_0/2=14.53~\mu {\rm S}\Box^{-1}$  in all cases. Note that for simplicity we show only one quadrant, since  $\phi(-x)=-\phi(x)$ . (b)–(d) The maximum as a function of (b) the sheet conductivity  $\sigma$  in the 2D half-plane ( $L=1~\mu {\rm m},~W=0.2~\mu {\rm m}$ ), (c) source-to-drain distance  $L~(\sigma=0.25G_0/2=9.69~\mu {\rm S}\Box^{-1},~W=0.2~\mu {\rm m})$ , and (d) distance from the ballistic channel  $W~(\sigma=0.25G_0/2,~L=1~\mu {\rm m})$ . The widths of the quasi-1D Ohmic channels are  $d=0.01~\mu {\rm m}$ .

A better overall agreement with  $\phi_{\text{ball}}$ , in particular for |x| > L, can be obtained by considering an Ohmic lower half-plane with sheet conductivity  $\sigma_{\text{lhp}} \equiv G_0/2$  in place of the ballistic channel (green profiles in Figs. 2 and 3). This boundary value problem can also be solved analytically [28] (Supplemental Material Note 3 [39]). Because of its 2D geometry, a distribution of current paths develops in the lower half-plane that mitigates the linear scaling of the resistance, the general property of all quasi-1D Ohmic channels that is in direct contrast with a ballistic channel. Thus, although the conducting lower half-plane does not represent a 1D channel geometrically and moreover is Ohmic, it turns out to be a reasonable proxy for a 1D ballistic channel in our contact geometry. With respect to experiments, this raises the question how the transport signature of a truly existing lower half-plane (e.g., the substrate terrace next to the edge of a quantum spin Hall insulator) can be distinguished from a ballistic edge channel. Here we note that, to be a good proxy, the lower half-plane has to have a sheet conductivity close to  $G_0/2$ , while any physical lower half-plane will have  $\sigma_{\rm lhp} \ll G_0/2$ , making it irrelevant for the transport problem. If in doubt,  $\sigma_{\rm lhp}$  can be measured independently to confirm that a transport signature similar to the one displayed by the orange symbols in Figs. 2 and 3 must be due to a ballistic edge channel.

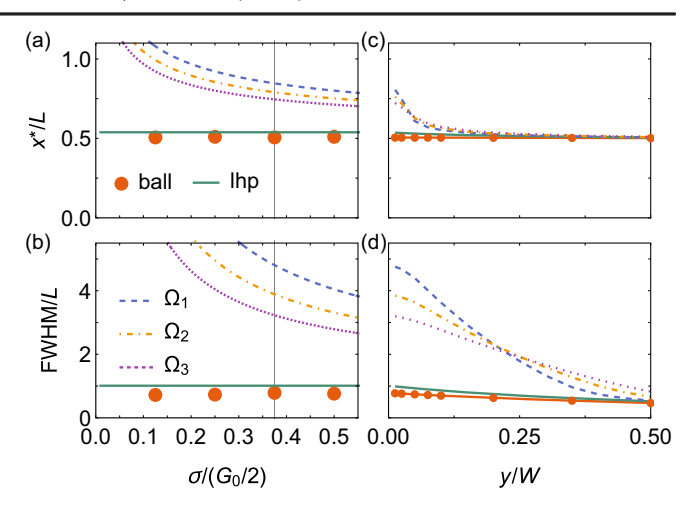


FIG. 3. (a),(c) Peak position  $x^*$  of the interface potential and (b),(d) corresponding FWHM, as a function of (a),(b) the sheet conductivity  $\sigma$  in the 2D half-plane and (c),(d) the distance y from the interface ( $\sigma=0.375G_0/2=14.53\,\mu\mathrm{S}\square^{-1}$ ), with  $L=1\,\mu\mathrm{m}$ ,  $W=0.2\,\mu\mathrm{m}$  in all cases. For the latter, the potential  $\Phi(x,y)$  was considered with y>0 fixed, instead of  $\phi(x)$ . Numerical solutions for the ballistic channel are shown by orange circles, analytic solutions of quasi-1D Ohmic channels (see Fig. 2 for conductivities)  $\Omega_1$  (dashed blue),  $\Omega_2$  (dash-dotted yellow), and  $\Omega_3$  (dotted purple), and a conducting lower half-plane (lhp) with  $\sigma_{\mathrm{lhp}}=G_0/2$  (solid green) are plotted for comparison.

Hallmark behavior of a ballistic channel—To pinpoint criteria which allow experimental identification of 1D ballistic transport, we explore some characteristic features of the interface potential  $\phi$ , keeping the total source-todrain current fixed. Figures 2(b), 3(a), and 3(b) show how the maximum  $\phi^*$  of the interface potential, its position  $x^*$ , and the full width at half maximum (FWHM) of the potential profile (the latter providing a measure of the decay at large distances) depend on the half-plane's sheet conductivity  $\sigma$ . The same conductivities of Ohmic channels as in Fig. 2(a) are employed. The scaling of  $\phi^*$  with  $\sigma$  is similar for all scenarios [Fig. 2(b)]. When analogously varying the source-to-drain distance L [Fig. 2(c)] and common distance to the ballistic channel W [Fig. 2(d)], we find a qualitatively different scaling behavior of  $\phi^*$  with L, increasing (decreasing) with L for the Ohmic (ballistic) channel. This reflects the qualitatively different resistive behavior of Ohmic and ballistic channels when changing the path lengths of conduction (see Supplemental Material Note 2 B for a more detailed discussion [39]). Moreover, all Ohmic channels display a much broader maximum [Fig. 3(b)] that is significantly displaced from the contact positions  $(x = \pm L/2)$  to larger x [Fig. 3(a)]. While the displacement quickly decays when moving away from the interface [Fig. 3(c)], the larger FWHM of Ohmic channels persists to rather large y [Fig. 3(d)], making the narrow FWHM a relevant and experimentally measurable signature that clearly differentiates ballistic from Ohmic channels.

Conclusion and outlook-We extended the standard Landauer approach to a ballistic channel in direct contact with a conducting half-plane to which source and drain contacts are applied. In this geometry, the current enters and leaves the ballistic channel via the half-plane in a spatially distributed manner. The potential at the interface between half-plane and ballistic channel displays distinct features compared to a quasi-1D Ohmic channel, such as a narrower maximum and a steeper decay at large distances, and opposite scaling of the maximum with the distance between the contacts. These features reflect the fundamental ballistic nature of the channel and can be used to identify ballistic channels in various topological materials experimentally, using potentiometry in multitip STM, for example. Our results thus widen the scope of multiprobe transport experiments to ascertain the ballistic nature of edge channels.

Our generalization of Landauer's theory to distributed injection can be applied to a wide range of contact geometries in a straightforward manner, by modifying the potential  $\Phi(x, y)$  on the left-hand side of Eq. (1) to match the appropriate boundary conditions in the 2D bulk region. The right-hand side of Eq. (1) can generally be applied for setups with a symmetric positioning for source and drain, for which  $\Delta x(\phi)$  follows naturally from symmetry considerations (Supplemental Material Note 2 [39]), while a generalization for asymmetric setups remains for future work. Furthermore, the filling condition for distributed injection can be extended to lithographic contacts that cover both 2D bulk and edge [19], by including the current that is directly injected and extracted via the contacts in addition to the distributed one when matching the density of states of the ballistic channel over the appropriate energy range. Thus, treating 1D ballistic edge channels in terms of the filling condition paves the way for a wide range of experimentally relevant setups with distributed injection, providing a valuable tool for the realistic treatment of transport in mixed-dimensional (2D-1D or even 3D-1D) systems [19,25,46].

Acknowledgments—The authors would like to thank Arthur Leis for insightful discussions. This work was supported by the German excellence cluster ML4Q (Matter and Light for Quantum Computing) and by the QuantERA grant MAGMA (by the German Research Foundation under Grant No. 491798118). K. M., F. L., and F. S. T. acknowledge the financial support by the Bavarian Ministry of Economic Affairs, Regional Development and Energy within Bavaria's High-Tech Agenda Project "Bausteine für das Quantencomputing auf Basis topologischer Materialien mit experimentellen und theoretischen Ansätzen" (Grant No. 07 02/686 58/1/21 1/22 2/23). K. M. acknowledges financial support by the German Federal Ministry of Education and Research (BMBF) via the Quantum Future project

"MajoranaChips" (Grant No. 13N15264) within the funding program Photonic Research Germany. C. W. acknowledges funding through the European Research Council (ERC-StG 757634 "CM3"). F. L. acknowledges funding by the Deutsche Forschungsgemeinschaft (DFG, German Research Foundation) within the Priority Programme SPP 2244 (Project No. 443416235), as well as the Emmy Noether Programme (Project No. 511561801). F. S. T. acknowledges funding by the Deutsche Forschungsgemeinschaft (DFG, German Research Foundation) through Coordinated Research Center CRC 1083, project ID 223848855.

Data availability—The data that support the findings of this article are openly available [42,43].

- [1] R. Landauer, Philos. Mag. 21, 863 (1970).
- [2] R. Landauer, Phys. Lett. 85A, 91 (1981).
- [3] R. Landauer, J. Math. Phys. (N.Y.) 37, 5259 (1996).
- [4] B. J. van Wees, H. van Houten, C. W. J. Beenakker, J. G. Williamson, L. P. Kouwenhoven, D. van der Marel, and C. T. Foxon, Phys. Rev. Lett. 60, 848 (1988).
- [5] R. de Picciotto, H. Stormer, L. Pfeiffer, K. Baldwin, and K. West, Nature (London) 411, 51 (2001).
- [6] S. Frank, P. Poncharal, Z. Wang, and W. de Heer, Science 280, 1744 (1998).
- [7] K. v. Klitzing, G. Dorda, and M. Pepper, Phys. Rev. Lett. 45, 494 (1980).
- [8] M. König, S. Wiedmann, C. Brüne, A. Roth, H. Buhmann, L. W. Molenkamp, X.-L. Qi, and S.-C. Zhang, Science 318, 766 (2007).
- [9] A. Roth, C. Brüne, H. Buhmann, L. W. Molenkamp, J. Maciejko, X.-L. Qi, and S.-C. Zhang, Science 325, 294 (2009).
- [10] I. Knez, R.-R. Du, and G. Sullivan, Phys. Rev. Lett. 107, 136603 (2011).
- [11] K. Lai, W. Kundhikanjana, M. A. Kelly, Z.-X. Shen, J. Shabani, and M. Shayegan, Phys. Rev. Lett. 107, 176809 (2011).
- [12] K. C. Nowack, E. M. Spanton, M. Baenninger, M. König, J. R. Kirtley, B. Kalisky, C. Ames, P. Leubner, C. Brüne, H. Buhmann, L. W. Molenkamp, D. Goldhaber-Gordon, and K. A. Moler, Nat. Mater. 12, 787 (2013).
- [13] K. M. Fijalkowski, N. Liu, P. Mandal, S. Schreyeck, K. Brunner, C. Gould, and L. W. Molenkamp, Nat. Commun. 12, 5599 (2021).
- [14] K. S. Novoselov, A. K. Geim, S. V. Morozov, D. Jiang, M. I. Katsnelson, I. V. Grigorieva, S. V. Dubonos, and A. A. Firsov, Nature (London) 438, 197 (2005).
- [15] C.-Z. Chang et al., Science 340, 167 (2013).
- [16] C. Pauly, B. Rasche, K. Koepernik, M. Liebmann, M. Pratzer, M. Richter, J. Kellner, M. Eschbach, B. Kaufmann, L. Plucinski, C. Schneider, M. Ruck, J. van den Brink, and M. Morgenstern, Nat. Phys. 11, 338 (2015).
- [17] F. Reis, G. Li, L. Dudy, M. Bauernfeind, S. Glass, W. Hanke, R. Thomale, J. Schäfer, and R. Claessen, Science 357, 287 (2017).

- [18] Z. Fei, T. Palomaki, S. Wu, W. Zhao, X. Cai, B. Sun, P. Nguyen, J. Finney, X. Xu, and D. H. Cobden, Nat. Phys. 13, 677 (2017).
- [19] S. Wu, V. Fatemi, Q. D. Gibson, K. Watanabe, T. Taniguchi, R. J. Cava, and P. Jarillo-Herrero, Science 359, 76 (2018).
- [20] Y. Shi, J. Kahn, B. Niu, Z. Fei, B. Sun, X. Cai, B. A. Francisco, D. Wu, Z.-X. Shen, X. Xu, D. H. Cobden, and Y.-T. Cui, Sci. Adv. 5, eaat8799 (2019).
- [21] M. Allen, Y. Cui, E. Yue Ma, M. Mogi, M. Kawamura, I. C. Fulga, D. Goldhaber-Gordon, Y. Tokura, and Z.-X. Shen, Proc. Natl. Acad. Sci. U.S.A. 116, 14511 (2019).
- [22] G. Lippertz, A. Bliesener, A. Uday, L. M. C. Pereira, A. A. Taskin, and Y. Ando, Phys. Rev. B 106, 045419 (2022).
- [23] G. M. Ferguson, R. Xiao, A. R. Richardella, D. Low, N. Samarth, and K. C. Nowack, Nat. Mater. 22, 1100 (2023).
- [24] T. Johnsen, C. Schattauer, S. Samaddar, A. Weston, M. J. Hamer, K. Watanabe, T. Taniguchi, R. Gorbachev, F. Libisch, and M. Morgenstern, Phys. Rev. B 107, 115426 (2023).
- [25] J. Baringhaus, M. Ruan, F. Edler, A. Tejeda, M. Sicot, A. Taleb-Ibrahimi, A.-P. Li, Z. Jiang, E. H. Conrad, C. Berger, C. Tegenkamp, and W. A. de Heer, Nature (London) 506, 349 (2014).
- [26] J. Aprojanz, I. Miccoli, J. Baringhaus, and C. Tegenkamp, Appl. Phys. Lett. 113, 191602 (2018).
- [27] S. Datta, Electronic Transport in Mesoscopic Systems, Cambridge Studies in Semiconductor Physics and Microelectronic Engineering (Cambridge University Press, Cambridge, England, 1995).
- [28] A. Leis, M. Schleenvoigt, K. Moors, H. Soltner, V. Cherepanov, P. Schüffelgen, G. Mussler, D. Grützmacher, B. Voigtländer, F. Lüpke, and F. S. Tautz, Adv. Quantum Technol. 5, 2200043 (2022).
- [29] P. Armagnat, A. Lacerda-Santos, B. Rossignol, C. Groth, and X. Waintal, SciPost Phys. 7, 031 (2019).
- [30] I. M. Flór, A. Lacerda-Santos, G. Fleury, P. Roulleau, and X. Waintal, Phys. Rev. B **105**, L241409 (2022).
- [31] B. Voigtländer, V. Cherepanov, S. Korte, A. Leis, D. Cuma, S. Just, and F. Lüpke, Rev. Sci. Instrum. 89, 101101 (2018).

- [32] F. Lüpke, S. Korte, V. Cherepanov, and B. Voigtländer, Rev. Sci. Instrum. 86, 123701 (2015).
- [33] S. Tang, C. Zhang, D. Wong, Z. Pedramrazi, H.-Z. Tsai, C. Jia, B. Moritz, M. Claassen, H. Ryu, S. Kahn *et al.*, Nat. Phys. **13**, 683 (2017).
- [34] F. Lüpke, D. Waters, A. D. Pham, J. Yan, D. G. Mandrus, P. Ganesh, and B. M. Hunt, Nano Lett. 22, 5674 (2022).
- [35] F. Lüpke, A. D. Pham, Y.-F. Zhao, L.-J. Zhou, W. Lu, E. Briggs, J. Bernholc, M. Kolmer, J. Teeter, W. Ko *et al.*, Phys. Rev. B **105**, 035423 (2022).
- [36] S. Yu, J. Deng, W. Liu, Y. Zhang, Y. Sun, N. Dhale, S. Li, W. Ma, Z. Wang, P. Wu, Z. Liang, X. Zhang, B. Lv, Z. Wang, Z. Wang, and X. Chen, Phys. Rev. X 14, 041048 (2024).
- [37] A. Leis, M. Schleenvoigt, V. Cherepanov, F. Lüpke, P. Schüffelgen, G. Mussler, D. Grützmacher, B. Voigtländer, and F. S. Tautz, Adv. Quantum Technol. 4, 2100083 (2021).
- [38] A. Leis, V. Cherepanov, B. Voigtländer, and F. S. Tautz, Rev. Sci. Instrum. 93, 013702 (2022).
- [39] See Supplemental Material at http://link.aps.org/supplemental/10.1103/l47r-plxq for details, which includes Refs. [40,41].
- [40] A. Prosperetti, *Advanced Mathematics for Applications* (Cambridge University Press, Cambridge, England, 2011).
- [41] Gradshteyn and Ryzhik, *Tables of Series, Products, and Integrals*, Vol. 1 (Verlag Harri Deutsch, Frankfurt am Main, 1981).
- [42] The code as well as numerical solutions presented in this article are openly available [43].
- [43] K. Moors, C. Wagner, H. Soltner, F. Lüpke, and F. S. Tautz, Data used in "Distributed Current Injection into a Onedimensional Ballistic Edge Channel", Jülich DATA, https:// doi.org/10.26165/JUELICH-DATA/PKSMCO (2025).
- [44] N. G. Leumer, D. M. Basko, R. A. Jalabert, D. Weinmann, and R. S. Whitney, Phys. Rev. B 110, 245402 (2024).
- [45] B. Weber, S. Mahapatra, H. Ryu, S. Lee, A. Fuhrer, T. C. G. Reusch, D. L. Thompson, W. C. T. Lee, G. Klimeck, L. C. L. Hollenberg, and M. Y. Simmons, Science 335, 64 (2012).
- [46] Y. Deng, Y. Yu, M. Z. Shi, Z. Guo, Z. Xu, J. Wang, X. H. Chen, and Y. Zhang, Science 367, 895 (2020).